A solution strategy to include the opening of the opercular slits in moving-mesh CFD models of suction feeding

Sam Van Wassenbergh[1,2]

[1]*Evolutionary Morphology of Vertebrates, Ghent University, Ledeganckstraat 35, B-9000 Gent, Belgium.*

[2] *Biology, Universiteit Antwerpen, Universiteitsplein 1, B-2610 Antwerpen, Belgium.*

Corresponding author email *sam.vanwassenbergh@ugent.be*

Running head: modelling suction feeding in fish

Synopsis

The gill cover of fish and pre-metamorphic salamanders has a key role in suction feeding by acting as a one-way valve. It initially closes to avoid an inflow of water through the gill slits, after which it opens to allow outflow of the water that was sucked through the mouth into the expanded buccopharyngeal cavity. However, due to the inability of analytical models (relying on the continuity principle) to calculate a fluid flow through a shape-and-size-changing cavity with two openings, stringent boundary conditions had to be used in previously developed mathematical models after the moment of valve opening. By solving additionally for momentum conservation, computational fluid dynamics (CFD) has the capacity to dynamically simulate these flows, but this technique also faces complications to model a transition from closed to open valves. Here, I present a relatively simple solution strategy to incorporate valve opening, exemplified in an axisymmetrical model of a suction-feeding sunfish in ANSYS Fluent software. By controlling viscosity of a separately defined fluid entity at the opercular cavity region, early inflow can be blocked (high viscosity assigned) and later outflow can be allowed (changing viscosity to that of water). Finally, by analysing the CFD solution obtained for the sunfish model, a few new insights in the biomechanics of suction feeding will be discussed.

Keywords: computational fluid dynamics, fish, hydrodynamics, biomechanics, prey capture

Introduction

Unidirectional suction feeding: the importance of caudal valve opening

Motion of water can carry along suspended food items considerably better than less viscous and less dense fluids such as air (Rubenstein and Koehl 1977). Nearly all aquatic feeders exploit these physical properties of water to capture prey (Herrel et al. 2012). Many of these are suction feeders: they generate a flow of water into a rapidly expanding oral cavity. This feeding mechanism overcomes that prey would be pushed away by the bow wave of the approaching predator (Dullemeijer 1994; Van Wassenbergh et al. 2010). It is therefore not surprising that suction is used to capture prey, often even highly evasive ones, by many aquatic vertebrates (e.g., Lauder 1983) as well as some predatory plants (Singh et al. 2011; Llorens et al. 2012).

Inside the head of aquatic anamniotes, distinct intra-oral volume entities are often defined. The buccal volume starts posterior of the mouth aperture, continues medial of the gill arches, and ends at the entrance of the oesophagus. Sometimes this cavity is referred to as the buccopharyngeal or oropharyngeal cavity (e.g. Liem 1984), where "buccal" or "oral" only refers to the portion lying anterior to the gill arches, and "pharyngeal" refers to the portion medial of the gill arches (Lauder 1983). In fish and gill-bearing salamanders, the intra-oral volume further consists of the left and right opercular cavities (parabranchial cavities in elasmobranchs) that form the space between the gills and their external covers. In ray-finned fishes, these external covers are formed by the opercular series of bones (opercula and subopercula) and more ventrally the branchiostegal membranes (consisting of mainly skin supported by long slender bones, the branchiostegal rays, attached to the hyoid).

It is generally accepted that it is sufficient to consider only a single functional unit as the expanding cavity during powerful suction feeding (e.g., van Leeuwen 1984; Muller and Osse 1984; Sanford

and Wainwright 2002; Van Wassenbergh et al. 2005) as the gill filaments then separate so that relatively large openings form through which water can pass with (probably) minimal resistance from the buccal cavity to the opercular cavities (Osse 1969; Alexander 1974; Muller et al 1982). Note, however, that not all of the sucked water will exit via one of the two opercular cavities, as often a large opening is formed between the hyoid arch and the first gill arch, the so-called hyoid shunt (van Leeuwen 1984).

This exit of water thought the operculo-branchiostegal slits (from this point onward referred to as the opercular slits) is of central importance to suction feeding performance (van Leeuwen 1984). It allows fish to engulf a volume of water much greater than the summed expansion of their buccal and opercular cavities (van Leeuwen, 1984; Higham et al. 2006; Kane and Higham 2014). Depending on swimming speed during suction feeding, the opening of the opercular slits occurs generally shortly before (e.g., a fast swimmer *Salmo gairdneri*; van Leeuwen 1984) or shortly after (e.g., a stationary suction feeder *Clarias gariepinus*; Van Wassenbergh et al. 2005) reaching maximal oral gape. As this instant of peak gape generally coincides with the instant at which the prey passes the mouth aperture (Muller and Osse 1984), an important part of the prey-capture process, namely the intra-oral transport of the prey while closing the mouth, takes place with opened caudal valves. Based on *in-vivo* flow visualisation of two species of centrarchid fishes (largemouth bass and bluegill sunfish), Day et al. (2005) estimated that a volume of water of about twice the expansion volume enters the mouth during prey capture. Furthermore, the estimated volume of water sucked in by *Salmo gairdneri* before the opening of the opercular slits was estimated to be only about 18% of the total volume of water flowing in through the mouth (van Leeuwen 1984). In addition, suction-feeding fish are able to maintain an inflow of water until the mouth is almost closed (Day et al., 2005; Higham et al., 2005), which likely decreases the prey's chances of escaping. This distinguishes fishes as unidirectional suction feeders from bidirectional suction feeders (e.g., snake-necked turtles: Aerts et al. 2001; pipid frogs: Carreño and Nishikawa

2010; post-metamorphic salamanders: Deban et al. 2001; seals: Marshall et al. 2014) that need to gently expel the sucked water through the narrowly opened mouth afterwards during the phase when the buccopharyngeal cavity slowly compresses to its initial volume.

From analytical to computational models of suction feeding

Despite the importance of the water sucked into the mouth after the opercular valves have opened, the final phase of suction feeding cannot be easily incorporated into the existing mathematical models of suction feeding hydrodynamics. Analytical models such as the expanding cone model (Muller et al 1982; Muller and Osse 1984), multi-cone models (Van Wassenbergh et al. 2006; Bishop et al. 2008), multi-elliptical-cylinder models (e.g., Drost and van den Boogaart 1986; Aerts et al. 2001; Van Wassenbergh et al. 2005; Roos et al. 2009) calculate flow velocities based on the principle of continuity (i.e., the incompressibility of water) applied to expanding volumes with a single opening: the mouth aperture. As soon as the opercular slits open, the equations of continuity alone are insufficient to determine in what direction and how fast the water is flowing. To surpass this limitation, Muller et al (1982) fixed the velocity of the water entering the mouth aperture (as a new boundary condition) from the moment of opercular slit opening. Ideally, however, the outflow dynamics could be simulated if also the equations of conservation of momentum of the water (Euler equations for inviscid flow or the Navier-Stokes equations for viscous flow) are solved for. This type of simulation can be performed using the method of computational fluid dynamics (CFD).

However, also with the help of modern, versatile, commercial CFD-simulation software it remains particularly challenging to tackle the dynamic transition from a closed to an open valve (e.g., Ramajo and Nigro 2008; Song et al 2010; Annerel et al 2011). One of the reasons for this is that the appearance of a new connection between fluid zones (in this case between the opercular cavity and the water outside of the fish) requires a change in boundary conditions, and hence the set-up of a new simulation. To model the full cycle of combustion in a car engine, for example, Ramajo and

Nigro (2008) solved the flow inside the cylinders and the exhaust ducts as two separate domains using commercial CFD software, while their custom-written FORTRAN functions fed solution of one domain as initial conditions in the other domain at the appropriate time. However, most industrial or biomedical engineering application focus either on the opening or closing process, thereby leaving a tiny opening in the valve at the beginning or end of the simulation (e.g., Srikanth and Bhasker 2009; Song et al. 2010; Wang et al. 2010; Dawy et al. 2013). A second factor of complexity is that valve action typically takes place in complex geometries with highly compliant walls involving strong fluid-structure interactions (Yoganathan et al. 2004; Annerel et al. 2011).

Moving-mesh CFD models (i.e. simulations with moving or shape-changing components in the domain) are of great promise to the analysis of suction feeding biomechanics (Van Wassenbergh and Aerts 2009). They already proved very useful to test fundamental principles in suction feeding biomechanics, such as the effect of the relative increase in viscous forces in the suction flows generated by suction feeders of small size (Drost et al 1988; Roos et al. 2011; Yaniv et al. 2014). These studies used models with symmetry about the long axis of the fish, but also fully three-dimensional morphologies can be used to dynamically simulate suction caused by programmatically prescribed head-surface deformations in CFD software (e.g., ANSYS Fluent) as shown in a recent study on suction feeding in a giant salamander (Heiss et al. 2013). The latter study demonstrates that recent advances in 3d-surface reconstruction of animals based on laser scanning or X-ray micro-computed tomography can be integrated with this type of biomechanical analysis.

Methods

In this article, I present a strategy to incorporate opercular valve outflow in moving-mesh CFD models of suction feeding. Doing so, my objective is not to aim for the most accurate possible model for opercular valve opening hydrodynamics using state-of-the-art approaches in fluid-structure interaction modelling (e.g., Annerel et al. 2011), but rather to provide a means to allow the

basic dynamics of a full expansion-compression cycle in a unidirectional suction feeder to be analysed with the smallest possible adjustments compared to existing moving-mesh CFD models mentioned above. The model will build upon an earlier version of an axially symmetric model in ANSYS Fluent of a suction-feeding sequence by the sunfish *Lepomis gibbosus* (total length = 75.7 mm) capturing a freely suspended bloodworm (Van Wassenbergh and Aerts 2009) (see Supplementary Video 1).

The first step in defining the model is to construct the model's initial geometry. The geometry of the sunfish model is based on the external and internal dimensions of the head at three positions along its length (Fig. 1A): at the front (mouth aperture), middle (just posterior of the eyes), and back (at the level of the dorsal part of the opercular slits) of the head. Spline curves fitted to control points at the external and internal contours at these three cross-sections formed the head of the model (Fig. 1B). The initial, internal dimensions of the jointed buccopharyngeal and opercular cavities were determined based on dorsoventral and lateral X-ray images of a specimen of which the mouth cavity was filled with a radio-opaque, Barium sulfate solution (see also Figure 9 of Roos et al. 2009). The body of the fish was modelled as a spindle of which the shape and size is controlled by 5 landmarks (Fig. 1B). A small gap of about 0.3 mm separated the head surfaces from the body surfaces at the level of the opercular slits. The prey was modelled as a sphere of 1 mm radius of which the distance to the centre of the mouth will match that of the bloodworm at the onset of head exapansion (Fig. 1). This geometry set-up was performed in Gambit 2.4.6 (Ansys Inc., Lebanon, USA).

A second step is to define the geometry of the fluid domain, to mesh this domain, and to assign boundary conditions. The key of the presented solution strategy lies in this section. Two lines were constructed between control nodes on the head and the body at the opercular gap (Fig. 2). This allows defining two fluid zones: (1) the main fluid zone surrounding head and body, and filling the buccopharyngeal cavity, and (2) the opercular fluid zone filling the narrow margin at the opercular

opening (Fig. 2). The physical properties assigned to the main fluid zone were that of normal water at 20°C (density 998.2 kg m^{-3}, viscosity 1.003 mPa s). In order to prevent flow through the opercular slits into the buccopharyngeal cavity at the instants when the opercular valves are closed in reality, the initial viscosity of the fluid in the opercular zone was set at a 200 times higher value (roughly in between water and honey). At the instant at which the valves are supposed to open, this initially much more viscous liquid changed its viscosity to that of water through a user-defined function (DEFINE_PROPERTY) as soon as the average pressure in the cells of the opercular fluid zone became positive in the previous time step. This opercular pressure was one of the output variables calculated after each time step (DEFINE_EXECUTE_AT_END). Declaring this variable as a global, static variable in the C-language user-defined function script allows it to be called for by the DEFINE_PROPERTY macro assigned to control the viscosity of the opercular cell zone. The reasoning behind the choice of the criterion of opening the opercular slits when pressure posterior inside the buccal cavity becomes positive is that valve opening is considered a predominantly passive, flow-driven phenomenon (Hughes and Shelton 1958). The remaining boundary conditions were the same as in previous moving-mesh suction models (Van Wassenbergh and Aerts 2009; Heiss et al. 2013; Yaniv et al. 2014): pressure outlets at the outer boundaries, and the no-slip condition enforced at the solid boundaries (head, body, and prey). The model was meshed with 100060 triangles (node spacing of 60 μm in the mouth cavity) using Gambit. Further information on user-defined function in ANSYS Fluent can be found in the ANSYS Fluent UDF Manual (e.g., version 14.5 published in 2012).

A third step is to prescribe the motion of the model to match the high-speed video as close as possible. Prey-capture kinematics were determined based on 23 anatomical landmarks (11 in lateral view, 12 in dorsal view; Fig. 1A) from which 2d-coordinates were measured frame-by-frame on the high-speed video images. Landmarks numbered 4, 7, and 8 (Fig. 1A) allowed the calculation of the instantaneous height and width at the front, middle and back of the head (Fig. 3A). The anterior-

posterior displacement of the eye landmark (landmark 6 in Fig. 1A) was used to calculate the axial translational velocity of the fish (Fig. 3B). The anterior-posterior displacement of the average of the coordinates of 3 landmarks on the bloodworm (2 tips and the approximate centre; numbered 1, 2, and 3 in Fig. 1A) was used to calculate the instantaneous velocity of the prey. Collision of the prey with the body was avoided by defining a minimal distance from prey to body, and overwriting the calculated velocity of the prey with the axial velocity of the fish as soon as this threshold was exceeded (see prey-collision-prevention buffer in Fig. 2B). Jaw protrusion was calculated as the distance between the tip of the premaxilla (landmark 5 in Fig. 1A) and the eye (or the centre between both eyes in dorsal view). To reduce manual coordinate-digitization noise, raw data were subjected to a fourth-order Butterworth filter (low-pass cut-off frequency of 20 Hz) designed to cause no phase shift (Winter 2004). First-order central differences in time were used to calculate velocities from displacements. To allow parameterisation of the model's kinematic input, sinusoidal functions were used to fit each profile with separate parameters (offset, amplitude and wavelength) defining the expansive and compressive parts of the profiles. Despite the differences between the kinematic profiles of width and height (Fig. 3D-F), only a single radial expansion profile can be used as model input per cross-section due to axial symmetry of the model. The best approximation of the instantaneous cross-sectional area is then to take the geometric mean (i.e., square root of the product) of instantaneous width and height to be used as the instantaneous radius of the model (Fig. 3D-F). Due to camera perspective and scaling imperfections, slight differences were also observed in the kinematic profiles of variables that could be measured both in lateral and dorsal view: prey velocity, fish velocity (Fig. 3B), and protrusion (Fig. 3C). The parametric input profiles were therefore fit to the arithmetic means of the lateral-view and dorsal-view variables (Fig. 3B-C).

Now that the expansion, protrusion and swimming kinematics are known (Fig. 3), they can be implemented in ANSYS Fluent to move the mesh. There are six degrees of freedom in the model

(Fig. 2B): (1) axial translation of the head and body, (2) radial translation of the mid-head point, (3) rotation of the anterior part of the head about the mid-head point, (4) rotation of the posterior part of the head about the mid-head point, (5) protrusion of the mouth, and (6) axial translation of the prey. Using relative rotation of the head parts allows a more natural flapping of the opercular valve. The independent radial expansions at the jaw tip and opercular tip region (Fig. 3D, 3F) were converted into rotations relative to the mid-head point. All these motions are controlled within the CFD-solver software by a user-defined function (DEFINE_GRID_MOTION) that was compiled, loaded, and assigned to the appropriate zones in the dynamic mesh panel of ANSYS Fluent.

Some of the simulated motions were not prescribed *a priori*, but are caused by the generated suction flows. Flow solutions were used to move the prey by the abovementioned user-defined function that summed the forces exerted at the surface of the prey (pressure forces and shear forces in the axial direction), and solved for acceleration using Newton's second law of motion (assuming a density equal to the surrounding water). Also the forward acceleration of the fish was solved for in this function by summing the hydrodynamic forces exerted at the head and body surfaces (and assuming the measured sunfish mass of 5 g). This forward acceleration during suction can be regarded as a fulfilment of the momentum conservation laws when a volume of water is accelerated posteriorly (see Muller and Osse 1984; Aerts et al. 2001). To do so, the fish was first accelerated to its observed swimming velocity (0.1 m s^{-1}; Fig. 3B) during the first 30 ms of the simulation, was moved at constant velocity for another 5 ms after which the axial acceleration of the fish was calculated with Newton's second law of motion.

The model was solved for 2400 time steps of 0.1 ms with the buccal expansion starting at time 0 (time step 400). The pressure-based solver (chosen to obtain fast-converging solutions) was used with a node-based Green-Gauss gradient treatment. The latter achieves a higher accuracy in unstructured triangular grids compared to the other options in ANSYS Fluent. The first-order implicit unsteady formulation option was used in the simulation because moving mesh simulations

(see above) currently only work with first-order time advancement. The standard pressure discretization scheme was used for the pressure calculation and a second-order upwind scheme was used for momentum equations. The pressure-velocity coupling was solved using the robust, default SIMPLE scheme. The latter is a discretization method that uses a relationship between velocity and pressure corrections to enforce mass conservation and to obtain the pressure field. Using a larger time step of 0.4 ms did not substantially influence the solution (e.g; only 1% difference in peak sub-ambient pressure in the opercular fluid zone, and 0.1% difference in peak flow speed at the mouth), indicating that 0.1 ms was more than sufficiently small. The software was set to move mesh nodes (spring-based smoothing algorithm; spring constant factor = 0.5; Laplace node relaxation = 1) and re-mesh (make new mesh for triangles smaller than 2×10^{-7} m and larger than 2×10^{-4} m) after every time step to adjust the internal nodes in response to the motion of the boundaries prescribed in the mesh-motion user-defined function. A mesh-convergence analysis was performed by comparing the solution with that of a much coarser mesh (9509 triangles, node spacing in the mouth cavity 2.66 times larger), which showed a 9% lower peak amplitude of opercular pressure, and a 0.4% higher peak of flow velocity at the mouth aperture (both peaking at the same time). This suggests that the used mesh was sufficiently fine.

A large set of output variables were calculated at the end of each time step by a user-defined function (DEFINE_EXECUTE_AT_END) hooked to Fluent. This set includes, amongst other, the peak and mean instantaneous flow velocities (axial and radial), the volumetric inflow rate or outflow rate, and mean pressure at the level of the mouth aperture and the opercular opening, instantaneous power and work requirements of the expansion.

Results and discussion

Model output and validation

The controlled modification of the viscosity in the opercular zone was successful in avoiding almost all of the flow that would otherwise enter the opercular cavity through the small gap at the gill slits of the presented sunfish model. In Figure 4, the model's output of flow in the opercular cell zone is compared with a case with no increased viscosity during the sub-ambient pressure stage of suction feeding. The difference is drastic: for example, peak inflow speed decreases from 0.30 m s^{-1} resulting in a backflow volume of 12% of the peak buccal volume, to 0.025 m s^{-1} with only about 1% of peak buccal volume sucked through the gill slits due to the 200-fold increase in viscosity (Fig. 4). In theory, this small amount of inflow could be eliminated by further increasing the viscosity. However, this caused the CFD solver to iterate to a diverging instead of converging solution at the time of switching between from the increased to the normal water viscosity, probably due to the too abrupt change in the physical properties of the system. The same problem also appeared when another, at first sight logical, modelling strategy was tried to cancel out opercular inflow: fixing the flow velocity in the opercular fluid zone (set to take the axial velocity of the fish), followed by a switch to a normally resolved flow velocity also failed to by solved by Fluent. Yet, if necessary, the remaining small amount of opercular inflow can be eliminated by narrowing the gap.

The strength of combining a moderately narrow gap with locally controlled fluid viscosity to prevent opercular inflow over the more traditional type of CFD-simulation of valve functioning by keeping a very tiny gap is further illustrated by a simulation performed with the opercular gap decreased from 0.3 mm to 0.02 mm (Fig. 4). Models with the original, larger gap combined with the locally increased viscosity outperformed the narrow-gap model with unmodified viscosity in preventing this inflow. The presented modelling strategy unnecessitates the local refinement of the mesh (and hence computational time increase) required for such a narrow gap. Furthermore, control over the close-to-open transition is simpler and also more versatile since it is independent of the expansion kinematics at the back of the head. If, for example, skin flaps at the edges of the opercular bones are still closing the opercular slits while the gill covers have started to abduct (a

situation common during respiration in fishes; Schmidt-Nielsen 1997), this situation can be modelled without including the actual motion of these skin flaps.

The accuracy of the model in predicting suction-feeding performance of the sunfish was assessed in two ways. Firstly, the velocity of the bloodworm measured from the high-speed video (average of landmarks 1-3 of Fig. 1A) was compared with the calculated velocity of the prey in the CFD-simulation. The model performed well at this aspect, as shown by the comparison displayed in Fig. 5. Secondly, the timing of opercular slit opening predicted by the model (time of transition from negative to positive pressure at the opercular region) was compared with that observed on the video images. The latter showed opening to occur approximately around the frame of a simulation flow time of 48 ms, while the model predicted opening to occur at 50.9 ms (Fig. 6). Consequently, these two tests show that prey-capture hydrodynamics are simulated with an accuracy that can be considered as high given the model's geometrical and kinematical simplifications.

Primary model output for flow patterns and pressure (Fig. 1A-B) generally corresponded well with the experimental data from the literature (see also Supplementary Videos 2 and 3). Two-dimensional flow velocities in the earth-bound frame in front of the mouth of 0.1 m s^{-1} have been calculated from flow visualisation for *L. gibbosus* (Lauder and Clark 1984). More recent particle image velocimetry studies on a closely related and morphologically similar species, *L. macrochirus*, showed velocities reaching up to 0.5 m s^{-1} (Fig. 2 in Day et al. 2005). Pressures (up to -300 Pa) were relatively low compared to measured values for sunfish (generally above -1000 Pa; Lauder 1980), but the small, unattached, dead prey I used for the video may not have elicited the most powerful suction act.

However, the model can still be improved at several aspects. Firstly, there is still a reasonably large amount of water blown out of the mouth during the phase of buccal compression (Fig. 7A, frames 80 and 100 ms; Fig. 7F, negative velocities at the mouth between t = 0.05 and 0.10 s), which

probably does not occur in reality (Lauder and Clark 1984). This may either be caused by overestimated buccal compression velocity, not having only the tip edges of the upper and lower jaws moving straight to each other to close the mouth, or due to a too narrow outflow opening. Secondly, the axial symmetry of the current model makes it unusable to answer certain functional-morphological questions. For example, the shape of the mouth is known to have an important effect on the external flow field (e.g. Skorczewski et al. 2012) and this shape generally differs from being perfectly planar and circular at least during some stage of suction feeding. Also biomechanical analyses of other aspects such as the lifting of the rostrum from the substrate to draw water under the body to assist benthic feeding in rays (Dean and Motta 2004; Wilga et al. 2012), the ventral deviation of the flow behind the mouth aperture towards the depressing hyoid apparatus as observed in catfish (Van Wassenbergh et al. 2007), or the dominating ventral outflow of water anterior of the first gill arch as noted for Rainbow trout (van Leeuwen 1984) call for full 3D models. Yet, the presented approach to model opercular valve opening with a programmatically controlled change in viscosity for separated fluid entities near the valves is by no means restricted in application to axisymmetric models.

Insights in suction-feeding mechanics

The strength of moving-mesh CFD models in biomechanical analyses is that virtually all aspects of the dynamics of the hydrodynamic action can be extracted from the solution during post-processing (e.g., Young et al. 2009; Zheng et al. 2013). This allows us to analyse aspects of suction mechanics that are not possible or too complex to solve analytically. Below, I will discuss two of these aspects that can help us to better understand the behaviour and functional morphology of suction feeders.

Suction-feeders suck themselves forward during suction generation (Muller et al. 1982; Aerts et al. 2001). Despite that the approaching motion of the suction feeder is a very important factor in determining prey-capture performance (e.g., van Leeuwen and Muller 1984; Holzman et al. 2008;

Kane and Higham 2011; Tran et al. 2010), this aspect of suction feeding mechanics has rarely been quantified (but see Aerts et al. 2001). The cause of this acceleration is (negative) pressure force pointing to the outside (i.e., into the water) of the forward-facing surfaces at the posterior end of the mouth cavity (corresponding to the anterior part of "body" in the presented model; Fig. 2). This causation can also be viewed in terms of momentum conservation (Aerts et al. 2001): the total momentum (mass x velocity) cannot change in a closed system on which no external forces and/or moments apply. The suction-induced backward momentum of the water will therefore be countered by forward momentum of the fish.

The presented CFD model showed that a relatively low-effort suction act (relatively low peak pressure of -0.3 kPa) by a sunfish accelerates the fish from 0.1 m s^{-1} to over 0.14 m s^{-1} in course of the time when suction pressure was generated. As note by Muller and Osse (1984), this effect will be larger in fish with a small body mass relative to suction power. The extreme example of animals making use of this effect are snake-necked turtles (*Chelodina*) in which only the extendible neck and head are taking all the forward momentum and shoot forward to overtake agile prey. Relatively large-headed, ambush-hunting fishes such as stonefish (Synanceiidae) or anglerfishes (*Antennarius*; Grobecker and Pietsch 1979) are also susceptible to make special use of this rapid forward acceleration due to suction, probably assisted by their locomotor system. The presented modelling strategy provides unique opportunities to study this aspect of mechanics of suction feeding in these fishes.

One of the consequences of this momentum-conservation effect is that the generated power by the suction-feeder's musculature during prey capture is converted into a change in kinetic energy of the sucked water, as well as a change in kinetic energy of the fish. In other words, as shown here for the sunfish model (Fig. 7I), only approximately half of the work done during suction was converted into suction flows as observed from the earth-bound frame of reference. A question that comes to mind is then: why don't many suction feeders bypass this effect, for example by holding on to the substrate with their fins. In this way, there is no closed system of water and suction feeder where momentum conservation applies as external, ground-reaction forces are in play, and the consequence would be that a larger fraction of muscle power results in

acceleration of water (and prey). There are two disadvantages to the situation of suction from a fixed position. Firstly, performing the same expansion without forward movement is energetically more costly, so that head expansion inevitably will be performed at lower speed from a fixed, standstill position. This comes down to the difference between the extremes of "compensatory suction" (i.e., wrapping the oral cavity volume around a parcel of water that remains motionless in the earth-bound frame of reference) and "inertial suction" (i.e., accelerating the water in the earth-bound frame of reference) as defined by Van Damme and Aerts (1997), or similarly to the effect of "translation pressure" to reduce expansion load as described by Muller (Muller et al. 1982). Secondly, by involving higher earth-bound-frame flow velocities and accelerations, the prey will be alerted earlier by the generated flow disturbances in the case of fixed-position suction feeding (Holzman and Wainwright 2009; Gemmell et al. 2013).

Secondly, CFD can help us to validate assumptions used in calculations based on empirical measurements. An important variable is suction power, which is typically defined as the power needed to expand the head against the hydrodynamic resistance (Van Wassenbergh et al. 2005). This variable can be linked back to the morphology and contractile mechanics of the muscles that generate suction, as muscle power is considered the main factor limiting head expansion speed (Aerts et al. 1987; Van Wassenbergh et al. 2005; Carroll and Wainwright 2009). Instantaneous suction power requirement can be estimated by multiplying instantaneous sub-ambient pressure inside the mouth cavity and the instantaneous rate of head-volume change (Carroll and Wainwright 2009). However, this estimate relies on several assumptions, as discussed in more detail in Van Wassenbergh et al. (2015). Ideally, local pressures and expansion rates at infinitesimally narrow, cross-sectional volume subdivisions of the mouth cavity should be used for this calculation, but usually (for practical reasons) only pressure at a single point is measured in the experiment. The comparison of a calculation of radial expansion power based on the finite volume mesh from the presented model (pressure and viscous force in the radial direction x radial velocity, then summing this for each surface mesh element of the head) with a single pressure point [example, mean pressure at the mouth region (Fig. 7E, blue curve) multiplied by the time derivative of head volume

change (based on Fig. 7D, sum of both curves)] is shown in Fig. 7H. There is definitely a general resemblance between the two curves, but it should be taken into account that both timing of the peak (0.024 ms versus 0.028 ms) and magnitude (3 mW versus 4.5 mW) can vary substantially because of the assumptions of the experimental-data-based calculation.

In conclusion, incorporating opercular slit opening and dynamically solving the motion of prey and fish due to suction add significantly to the prospective of CFD as a tool to study the functional morphology and biomechanics of suction feeders. The option to change the kinematic or morphological input parameters of the presented model has not been explored in the current article, but can potentially be used to explore the mechanical consequences of the wide variety of morphology and feeding kinematics observed in nature.

References

Aerts P, Osse JWM, Verraes W. 1987. Model of jaw depression during feeding in Astatotilapia elegans (Teleostei: Cichlidae): mechanisms for energy storage and triggering. J Morphol 194: 85-109.

Aerts P, Van Damme J, Herrel A. 2001. Intrinsic mechanics and control of fast cranio-cervical movements in aquatic feeding turtles. Amer Zool 41: 1299-1310.

Alexander R McN. 1974. Functional design in fishes. Hutchinson University Library London, UK.

Annerel S, Claessens T, Van Ransbeeck P, Segers P, Verdonck P and Vierendeels J. 2011. State-of-the-art methods for the numerical simulation of aortic BMHVs. Aortic valve. ed.:Ying-Fu Chen; Chwan-Yau Luo. InTech, 2011.

Bishop KL, Wainwright PC, Holzman R. 2008. Anterior to posterior wave of buccal expansion in suction feeding fish is critical for optimizing fluid flow velocity profile. J R Soc Interface 5:1309-1316.

Carreño CA, Nishikawa KC. 2010. Aquatic feeding in pipid frogs: the use of suction for prey capture. J Exp Biol 213: 2001-2008.

Carroll AM, Wainwright PC. 2009. Energetic limitations on suction feeding performance in Centrarchidae. J Exp Biol 212: 3241-3251.

Dawy A, Sharara A, Hassan A. 2013. A numerical investigation of the incompressible flow through a butterfly valve using CFD. Int J Emerg Tech Adv Eng 3, 1-7.

Day SW, Higham TE, Cheer AY, Wainwright PC. 2005. Spatial and temporal patterns of water flow generated by suction-feeding bluegill sunfish *Lepomis macrochirus* resolved by Particle Image Velocimetry. J Exp Biol 208: 2661-2671.

Dean MN, Motta PJ. 2004. Feeding behavior and kinematics of the lesser electric ray, Narcine brasiliensis (Elasmobranchii: Batoidea). Zoology 107: 171–189.

Deban SM, Wake DB. 2000. Aquatic feeding in salamanders. In Feeding: form, function and evolution in tetrapod vertebrates (ed. K Schwenk), pp. 65–94. San Diego, CA: Academic Press.

Drost MR, Muller M, Osse J. 1988. A quantitative hydrodynamical model of suction feeding in larval fishes: the role of frictional forces. Proc R Soc B 234: 263–281.

Drost MR, van den Boogaart JGM. 1986. A simple method for measuring the changing volume of small biological objects, illustrated by studies of suction feeding by fish larvae and of shrinkage due to histological fixation. J Zool, Lond 209: 239-249.

Dullemeijer P. 1994 Conclusion: A general theory for feeding mechanics? In: *Advances in Comparative and Environmental Physiology, Vol. 18* (Bels, V.L., Chardon, M. and Vandewalle P. eds). Springer Verlag: Berlin Heidelberg.

Gemmell BJ, Adhikari D, Longmire EK. 2013. Volumetric quantification of fluid flow reveals fish's use of hydrodynamic stealth to capture evasive prey. J R Soc Interface 11: 20130880.

Grobecker DB, Pietsch TW. 1979. High-speed cinematographic evidence for ultrafast feeding in antennariid anglerfishes. Science 205: 1161-1162.

Heiss E, Natchev N, Gumpenberger M, Weissenbacher A, Van Wassenbergh S. 2013. Biomechanics and hydrodynamics of prey capture in the Chinese giant salamander reveal a high-performance jaw-powered suction mechanism. J R Soc Interface 10, 20121028.

Herrel A, Van Wassenbergh S, Aerts P. June 2012. Biomechanical studies of food and diet selection. In: eLS. Chichester: John Wiley and Sons, Ltd.

Higham TE, Day SW, Wainwright PC. 2005. Sucking while swimming: evaluating the effects of ram speed on suction generation in bluegill sunfish (*Lepomis macrochirus*) using digital particle image velocimetry. J Exp Biol 208: 2653-2660.

Higham TE, Day SW, Wainwright PC. 2006. Multidimensional analysis of suction feeding performance in fishes: fluid speed, acceleration, strike accuracy and the ingested volume of water. J Exp Biol 209: 2713-2725.

Holzman R, Day SW, Mehta RS, Wainwright PC. 2008. Jaw protrusion enhances forces exerted on prey by suction feeding fishes. J R Soc Interface 5:1445-1457.

Holzman R, Wainwright PC. 2009. How to surprise a copepod: strike kinematics reduce hydrodynamic disturbance and increase stealth of suction-feeding fish. Limnol Oceanogr 54:2201-2212.

Hughes GM, Shelton G. 1958. The mechanism of gill ventilation in three freshwater teleosts. J Exp Biol 35:807-823.

Kane EA, Higham TE. 2011. The integration of locomotion and prey capture in divergent cottid fishes: functional disparity despite morphological similarity. J Exp Biol 214:1092-1099.

Kane EA, Higham TE. 2014. Modelled three-dimensional suction accuracy predicts prey capture success in three species of centrarchid fishes. J R Soc Interface 11: 20140223.

Lauder, GVJr. 1980. Evolution of the feeding mechanism in primitive actinopterygian fishes: a functional anatomical analysis of *Polypterus*, *Lepisosteus*, and *Amia*. J Morphol 163:283-317.

Lauder GV. 1983. Food capture. In: *Fish Biomechanics*, edited by P.W. Webb and D. Weihs, Praeger Publishers, New York. Pp. 280-311.

Lauder GV, Clark BD. 1984. Water flow patterns during prey capture by teleost fishes. J Exp Biol 113:143-150.

Liem KF. 1984. The muscular basis of aquatic and aerial ventilation in the air-breathing teleost fish *Channa*. J Exp Biol 113:1-18.

Llorens C, Argentina M, Bouret Y, Marmottant P, Vincent O. 2012. A dynamical model for the *Utricularia* trap. J R Soc Interface 7:3129-3139.

Marshall CD, Wieskotten S, Hanke W, Hanke FD, Marsh A, Kot B and Dehnhardt G. 2014. Feeding kinematics, suction, and hydraulic jetting performance of harbor seals (Phoca vitulina). PLoS One 9:e86710.

Muller M, Osse JWM, Verhagen JHG. 1982. A quantitative hydrodynamic model of suction feeding in fish. J Theor Biol 95: 49-79.

Muller M, Osse JWM. 1984. Hydrodynamics of suction feeding in fish. Trans Zool Soc Lond 37: 51–135.

Osse JWM. 1969. Functional morphology of the head of the perch (Perca fluviatilis L.): an electromyographic study. Neth J Zool 19:289-392.

Ramajo DE, Nigro NM. 2008. Numerical and experimental in-cylinder flow study in a 4-valve spark ignition engine. Mecánica Computacional 27:181-205.

Roos G, Van Wassenbergh S**,** Herrel A, Aerts P. 2009. Kinematics of suction feeding in the seahorse *Hippocampus reidi*. J Exp Biol 212: 3490-3498.

Roos G, Van Wassenbergh S, Aerts P, Herrel A, Adriaens D. 2011. Effects of snout dimensions on the hydrodynamics of suction feeding in juvenile and adult seahorses. J Theor Biol 269: 307-317.

Rubenstein DI and Koehl MAR. 1977. The mechanisms of filter feeding: some theoretical considerations. Amer Natur 111: 981-994.

Sanford CPJ, Wainwright PC. 2002. Use of sonomicrometry demonstrates link between prey capture kinematics and suction pressure in largemouth bass. J Exp Biol 205: 3445-3457.

Schmidt-Nielsen K. 1997. Animal physiology: adaptation and environment. 5th edition. Cambridge University Press, Cambridge.

Skorczewski T, Cheer A, Wainwright PC. 2012. The benefits of planar circular mouths on suction feeding performance. J R Soc Interface 9:1767-1773.

Singh AK, Prabhakar S, Sane SP. 2011. The biomechanics of fast prey capture in aquatic bladderworts. Biol Lett 7: 547-550.

Song XG, Wang L, Park YC.2010. Transient analysis of a spring-loaded pressure safety valve using computational fluid dynamics (CFD). J Press Vess-T ASME 132: 054501

Srikanth C, Bhasker C. 2009. Flow analysis in valve with moving grids through CFD techniques. Adv Eng Softw 40: 193-201

Tran HQ, Mehta RS, Wainwright PC. 2010. Effects of ram speed on prey capture kinematics of juvenile Indo-Pacific tarpon, Megalops cyprinoides. Zoology 113:75-84.

Van Damme J, Aerts P. 1997. Kinematics and functional morphology of aquatic feeding in Australian snake-necked turtles (Pleurodira; Chelodina). J Morphol 233:113-125.

van Leeuwen JL, Muller M. 1984. Optimum sucking techniques for predatory fish. Trans Zool Soc Lond 37:137-169.

van Leeuwen JL. 1984. A quantitative study of flow in prey capture by Rainbow trout, *Salmo gairdneri* with general consideration of the actinopterygian feeding mechanism. Trans Zool Soc Lond 37: 171-227.

Van Wassenbergh S, Aerts P, Herrel A. 2005. Scaling of suction-feeding kinematics and dynamics in the African catfish, *Clarias gariepinus*. J Exp Biol 208: 2103-2114.

Van Wassenbergh S, Aerts P, Herrel A. 2006. Hydrodynamic modeling of aquatic suction performance and intra-oral pressures: limitations for comparative studies. J R Soc Interface 3: 507-514.

Van Wassenbergh S, Herrel A, Adriaens D, Aerts P. 2007. No trade-off between biting and suction feeding performance in clariid catfishes. J Exp Biol 210: 27-36.

Van Wassenbergh S, Brecko J, Aerts P, Stouten I, Vanheusden G, Camps A, Van Damme R, Herrel A. 2010. Hydrodynamic constraints on prey-capture performance in forward-striking snakes. J R Soc Interface 7: 773-785

Van Wassenbergh S, Day SW, Hernández P, Higham TE, Skorczewski T. 2015. Suction power output and the inertial cost of rotating the neurocranium to generate suction in fish. J Theor Biol 372: 159-167.

Wang L, Song XG, Park YC. 2010. Dynamic analysis of three-dimensional flow in the opening process of a single-disc butterfly valve. Proc Inst Mech Eng C J Mech Eng Sci 224: 329-336.

Wilga CD, Maia A, Nauwelaerts S, Lauder GV. 2012. Prey handling using whole-body fluid dynamics in batoids. Zoology 115: 47–57.

Winter DA. 2004. Biomechanics and Motor Control of Human Movement, 3rd edition. USA, John Wiley & Sons.

Yaniv S, Elad D, Holzman R. 2014. Suction feeding across fish life stages: flow dynamics from larvae to adults and implications for prey capture. J Exp Biol 217:3748-3757.

Yoganathan AP, He Z, Jones SC. 2004. Fluid mechanics of heart valves. Annu Rev Biomed Eng 6:331-362

Young J, Walker SM, Bomphrey RJ, Taylor GK, Thomas ALR. 2009. Details of insect wing design and deformation enhance aerodynamic function and flight efficiency. Science 325: 1549-1552.

Zheng L, Hedrick TL, Mittal R. 2013. Time-varying wing-twist improves aerodynamic efficiency of forward flight in butterflies. PLoS ONE 8(1): e53060.

Funding

Support for participation in this symposium was provided by the Division of Comparative Biomechanics of the Society for Integrative and Comparative Biology. This work was conducted as a part of the Suction Feeding Biomechanics Working Group at the National Institute for Mathematical and Biological Synthesis, sponsored by the National Science Foundation through NSF Award #DBI-1300426, with additional support from The University of Tennessee, Knoxville. CFD software and hardware was funded by grants from the Fund for Scientific Research Flanders (FWO) Grant 1516008N00 and the University of Antwerp (BOF/KP 24346). This study is additionally funded by the FWO project G014911N.

Figure Legends

Figure 1. Geometry of the axially symmetric model of suction feeding in the sunfish *Lepomis gibbosus*. Outlines of the sunfish and prey (bloodworm) in (**A**) show the position of the numbered anatomical landmarks from which position coordinates were determined for each high-speed video frame. The basic geometry of the model parameterized by the positions of 20 control points is shown in (**B**). Graphical 3d-reconstructions of the model after rotation about the symmetry axis are illustrated both mid-sagittally sectioned (**C**, top) and in external view (**C**, bottom). Scale bar, 20 mm.

Figure 2. CFD domain indicating the boundary conditions (**A**) and kinematic input variables included in the grid deformation functions (**B**). Note that the fluid zone is subdivided into two parts in order to assign different physical properties to the fluid adjacent to the gill cover. Here, the internal boundary of the opercular fluid zone (by approximation) transects the branchial arches, but this choice was arbitrary.

Figure 3. Kinematics of the modelled prey-capture event. The meaning of the kinematic variables derived from the anatomical landmarks (Fig. 1A) is illustrated in (**A**). Smoothed kinematic profiles from corresponding lateral-view (dotted lines) and dorsal-view variables (dashed lines) are given in each graph, together with either the arithmetic (**B-C**) or geometric mean (**D-F**) (thin full line; online in red). The expansion variables shown in graphs (**C-F**) are indicated by Δ, meaning that these are instantaneous distances minus the distance at rest.

Figure 4. Performance of different settings for initial viscosity of the opercular fluid in the CFD model in preventing inflow during suction (shaded area), and comparison with a model using only a strongly decreased opercular gap size (mesh zoomed in on the opercular gap shown at the top). The dotted line represents model output without modified viscosity ($\mu = 1.003\ 10^{-3}$ Pa s), the dashed line with 50 times increased initial viscosity ($\mu = 50 \times 10^{-3}$ Pa s), the full line (online in red) with 200 times increased viscosity ($\mu = 200 \times 10^{-3}$ Pa s), and the dash-dot line (online in blue) with the narrowed opercular gap without modified viscosity. Scale bar, 2.5 mm.

Figure 5. Comparison of predicted prey velocity from CFD and the observed velocity of the bloodworm (using the average position of the landmarks 1,2 and 3 of Fig. 1A).

Figure 6. First video frame from the modelled prey-capture sequence that shows opening of the gill slits (flow time = 48 ms). The timing of this event is predicted reasonably well by the model: the calculated time at which the opercular pressure becomes positive was 50.9 ms).

Figure 7. CFD-model results. Flow velocity magnitudes (colours, see legend on top) and directions (arrowheads), and gauge pressures (colours, see legend on top) are given in respectively (**A**) and (**B**) for 20 ms intervals of the simulation (see also Supplementary Videos 2 and 3). Temporal profiles of several important variables are given in the right column of graphs (**C-I**). The grey background indicates the phase of opened opercular slits in these graphs. Note that the opercular fluid zone refers to the region as defined in Fig. 2A. Mean values from the mouth aperture plane are taken from cell data for the anteriormost 5% of the head. In (**I**) work required from the feeding musculature is defined as negative, while work outputs (kinetic energy increases) are defined as positive.

Supplementary materials legends:

Supplementary Video 1 (.mpg, 1.4 MB): Slow-motion replay of the lateral-view and dorsal-view video of a juvenile *Lepomis gibbosus* capturing a bloodworm, the event mimicked by the presented CFD model.

Supplementary Video 2 (.mpg, 1.1 MB): Axial velocity output of the CFD model (real-time duration = 0.24 s)

Supplementary Video 3 (.mpg, 1.0 MB): Pressure output of the CFD model (real-time duration = 0.24 s).

Figure 1

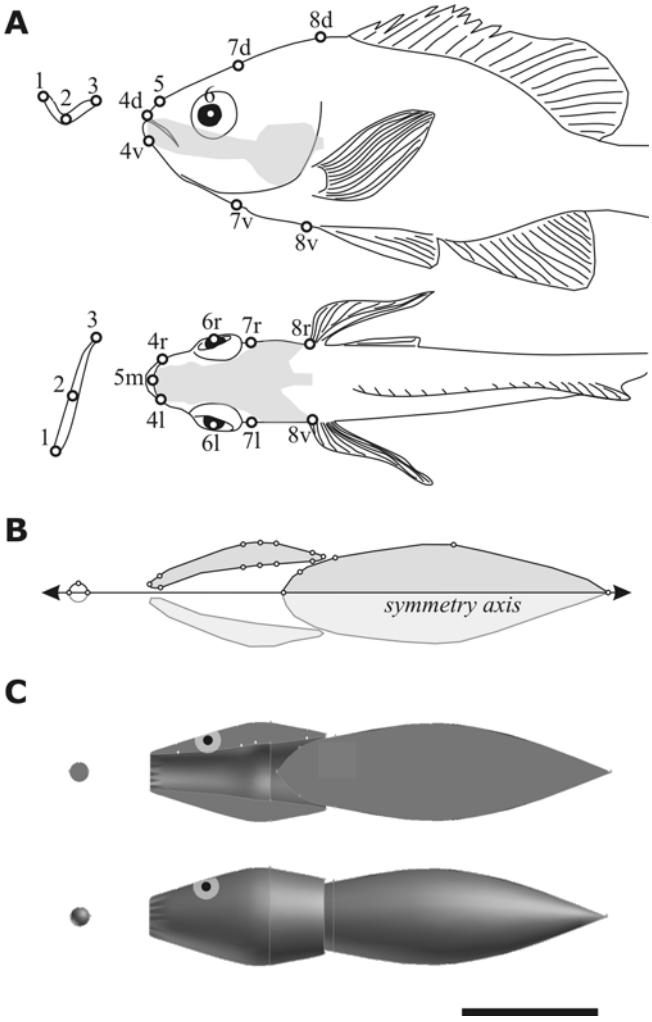
A
1
2
3
4d
5
6
7d
8d
4v
7v
8v
3
2
1
4r
5m
4l
6r
7r
8r
6l
7l
8v
B
symmetry axis
C

Figure 2

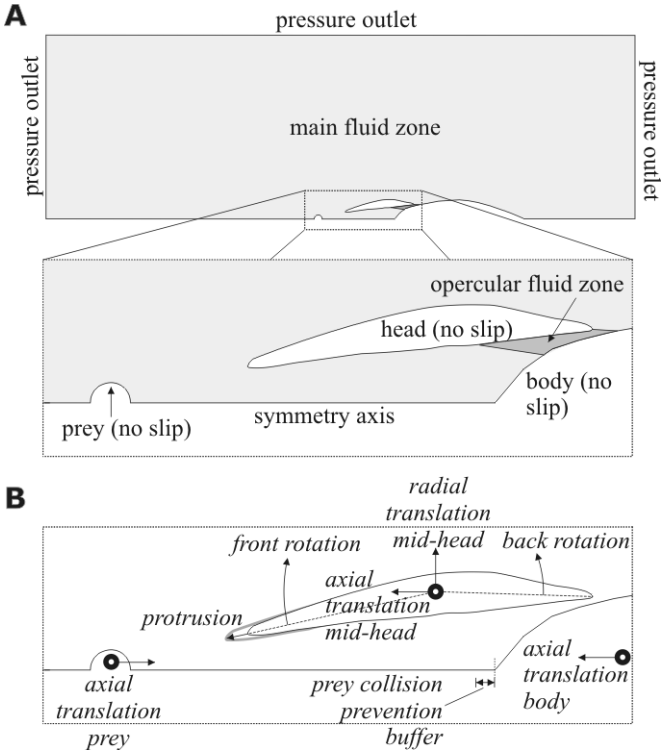
A
pressure outlet
pressure outlet
main fluid zone
pressure outlet
opercular fluid zone
head (no slip)
body (no slip)
prey (no slip)
symmetry axis
B
radial translation mid-head
front rotation
back rotation
axial translation mid-head
protrusion
axial translation prey
prey collision prevention buffer
axial translation body

Figure 3

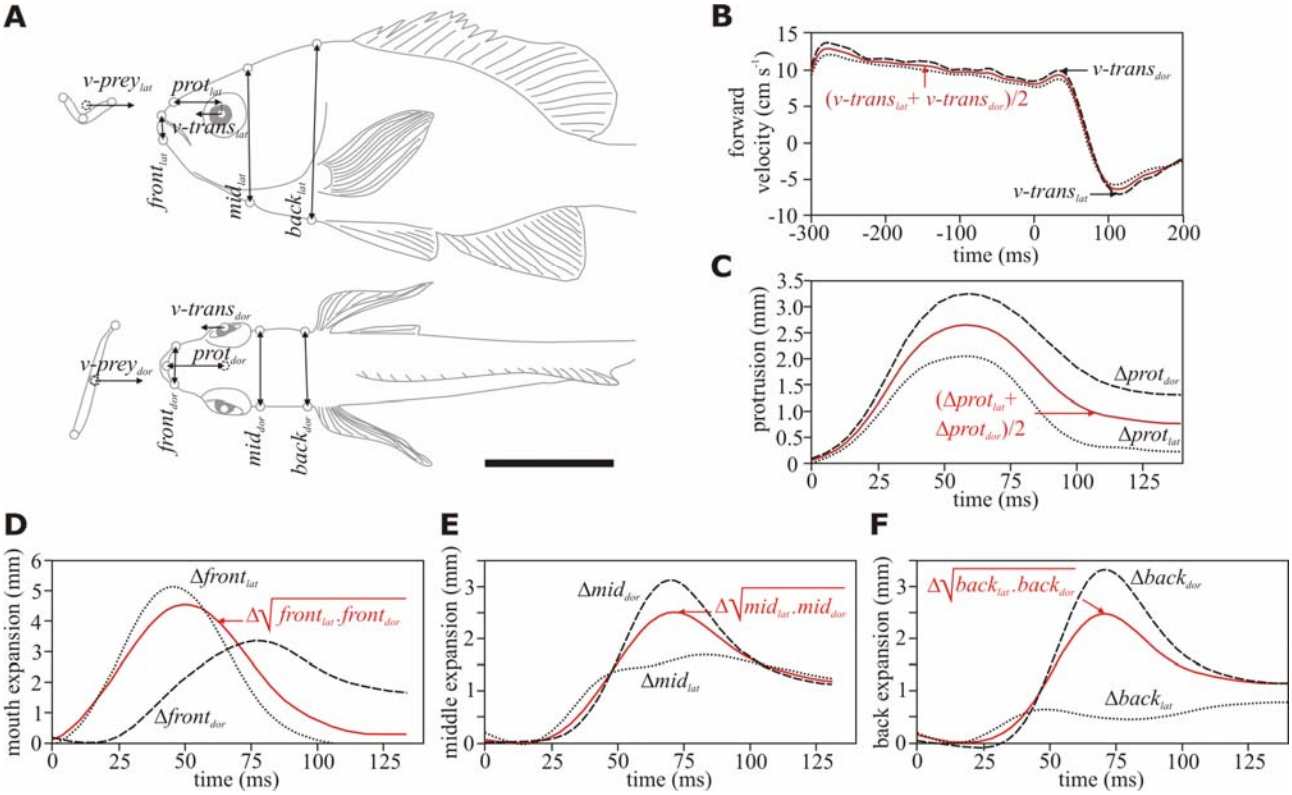
A
v-prey_lat
prot_lat
v-trans_lat
front_lat
mid_lat
back_lat
v-trans_dor
v-prey_dor
prot_dor
front_dor
mid_dor
back_dor
B
forward velocity (cm s-1)
(v-trans_lat+ v-trans_dor)/2
v-trans_dor
v-trans_lat
time (ms)
C
protrusion (mm)
Δprot_dor
(Δprot_lat+ Δprot_dor)/2
Δprot_lat
time (ms)
D
mouth expansion (mm)
Δfront_lat
Δ√(front_lat.front_dor
Δfront_dor
time (ms)
E
middle expansion (mm)
Δmid_dor
Δ√(mid_lat.mid_dor
Δmid_lat
time (ms)
F
back expansion (mm)
Δ√(back_lat.back_dor
Δback_dor
Δback_lat
time (ms)

Figure 4

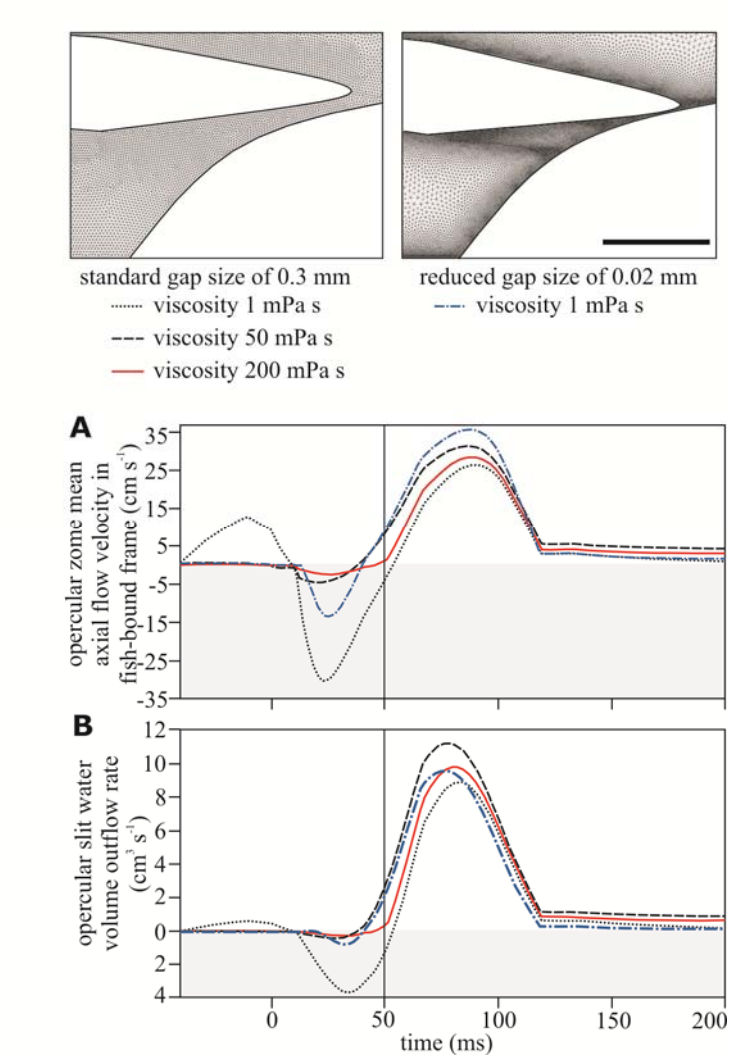
standard gap size of 0.3 mm
viscosity 1 mPa s
viscosity 50 mPa s
viscosity 200 mPa s
reduced gap size of 0.02 mm
viscosity 1 mPa s
A
opercular zome mean axial flow velocity in fish-bound frame (cm s-1)
35
25
15
5
-5
-15
-25
-35
B
opercular slit water volume outflow rate (cm3 s-1)
12
10
8
6
4
2
0
2
4
0
50
100
150
200
time (ms)

Figure 5

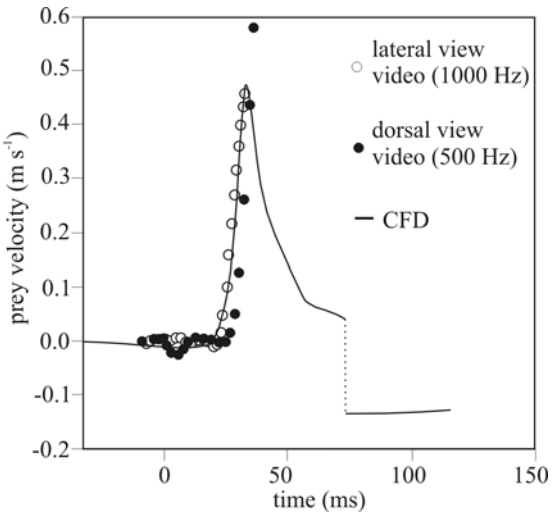
0.6
0.5
0.4
0.3
0.2
0.1
0.0
-0.1
-0.2
prey velocity (m s-1)
0
50
100
150
time (ms)
lateral view
video (1000 Hz)
dorsal view
video (500 Hz)
CFD

Figure 6

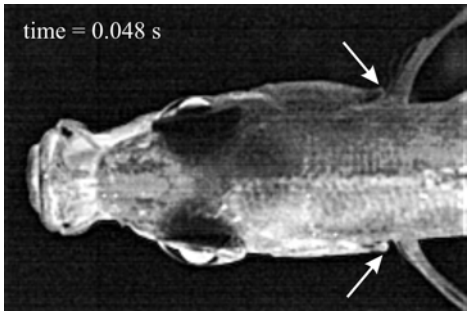

Figure 7

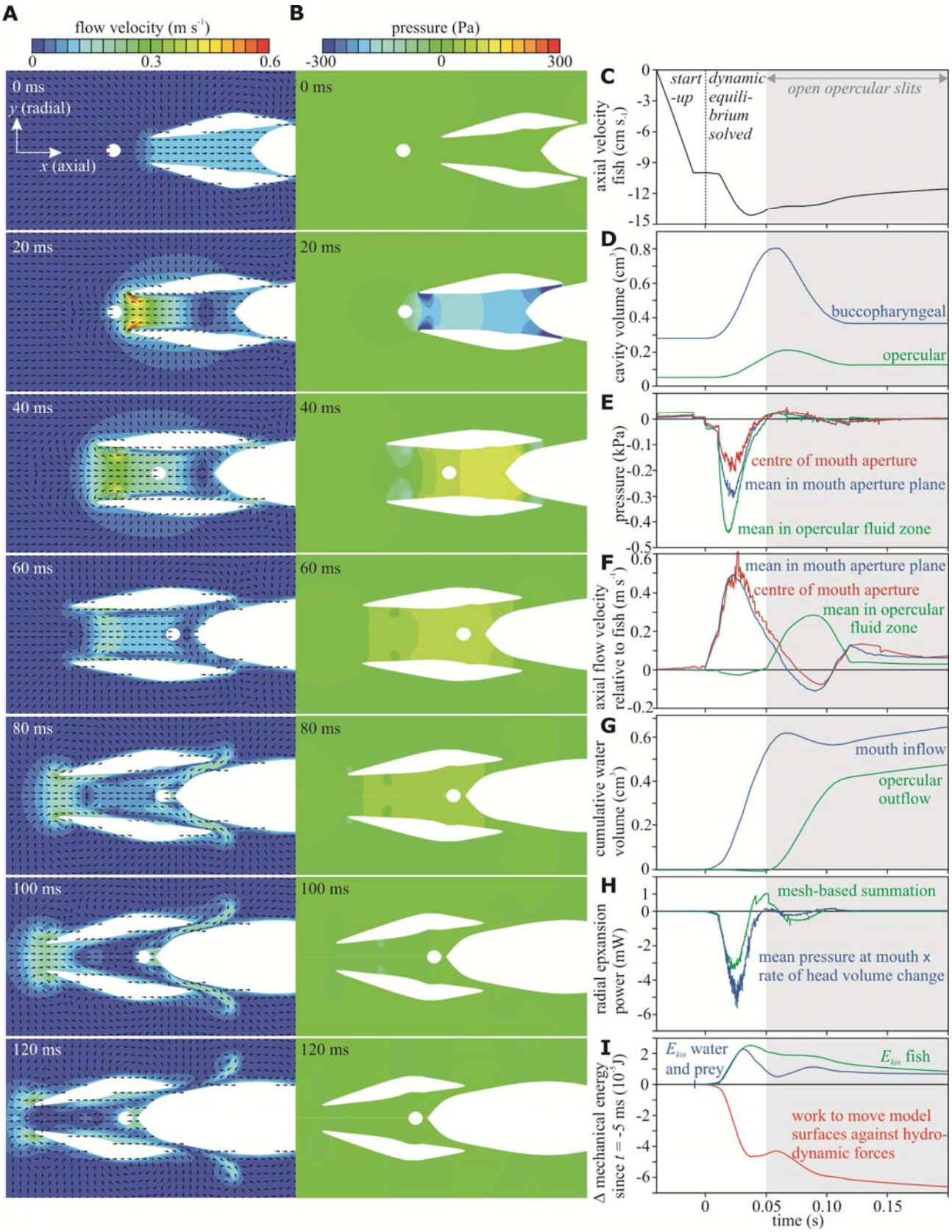
A
flow velocity (m s-1)
0
0.3
0.6
B
pressure (Pa)
-300
0
300
0 ms
y (radial)
x (axial)
20 ms
40 ms
60 ms
80 ms
100 ms
120 ms
C
start -up
dynamic equili-brium solved
open opercular slits
axial velocity fish (cm s-1)
D
cavity volume (cm3)
buccopharyngeal
opercular
E
pressure (kPa)
centre of mouth aperture
mean in mouth aperture plane
mean in opercular fluid zone
F
axial flow velocity relative to fish (m s-1)
mean in mouth aperture plane
centre of mouth aperture
mean in opercular fluid zone
G
cumulative water volume (cm3)
mouth inflow
opercular outflow
H
radial expansion power (mW)
mesh-based summation
mean pressure at mouth x rate of head volume change
I
Δ mechanical energy since t = -5 ms (10-5 J)
Ekin water and prey
Ekin fish
work to move model surfaces against hydro-dynamic forces
0
0.05
0.10
0.15
time (s)